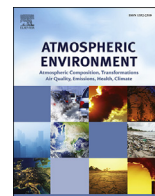




Contents lists available at ScienceDirect

Atmospheric Environment

journal homepage: www.elsevier.com/locate/atmosenv

Ozone, water vapor, and temperature anomalies associated with atmospheric blocking events over Eastern Europe in spring - summer 2010

S.A. Sitnov^{a,*}, I.I. Mokhov^{a,b}, A.R. Lupo^c^a A.M. Obukhov Institute of Atmospheric Physics, Russian Academy of Sciences, Moscow, Russia^b Lomonosov Moscow State University, Moscow, Russia^c Department of Atmospheric Sciences, University of Missouri, Columbia, MO, USA

HIGHLIGHTS

- Atmospheric blocking influences regional atmospheric composition.
- Water vapor increases in the troposphere and stratosphere over the blocks.
- Negative total column ozone anomalies dominate within the blocking domains.
- The ozone and water vapor anomalies is due mainly to atmospheric dynamics.
- Interconnection of blocking anticyclone with stationary Rossby wave.

ARTICLE INFO

Article history:

Received 26 November 2016

Received in revised form

31 May 2017

Accepted 2 June 2017

Available online 3 June 2017

Keywords:

Ozone

Water vapor

Temperature

Atmospheric blocking

AIRS

ABSTRACT

Using data from the AIRS satellite instrument (V6, L3), ozone, water vapor (WV), and temperature anomalies associated with the relatively short spring atmospheric blocking event and anomalously prolonged summer block over European Russia (ER) in 2010 are analyzed. Within the domain of the blocking anticyclones, negative total column ozone (TCO) anomalies and positive total column water vapor (TCWV) anomalies reaching the values of -25 and -32 Dobson Units (DU) and 10 and 11 kg m^{-2} during the spring and summer blocks are observed, respectively. Conversely, within the regions adjacent to the anticyclones to the west and east, positive TCO anomalies (77 and 45 DU) and negative TCWV anomalies (-3 and -4 kg m^{-2}) are found. These TCO and TCWV anomalies are conditioned by the regional atmospheric circulation associated with the strong omega-type blocking. The TCO deficit and TCWV surplus within the atmospheric blocking domain are explained primarily by the poleward advection of subtropical air with low TCO and high TCWV content and tropopause uplift. The TCO and TCWV anomalies are also associated with quasi-stationary Rossby wave trains that accompanied these blocking events. An analysis of the anomaly vertical structure shows that the marked TCO decrease is primarily due to the lower stratospheric ozone decrease, while the strong TCWV increase is mainly the result of an increase of lower tropospheric WV content. The possible role of photochemical ozone destruction in the lower stratosphere due to WV advection within the blocked regions is also discussed. Vertical profiles of the thermal anomalies during both atmospheric blocking events reveal dipole-like structures characterized by positive temperature anomalies in the troposphere and negative anomalies in the lower stratosphere.

© 2017 Elsevier Ltd. All rights reserved.

1. Introduction

Atmospheric blocking is associated with the formation of a strong stationary anticyclone, which impedes the westerly transfer of air masses in the mid-latitude troposphere (Rex, 1950). It is believed that block formation is closely related to nonlinear

* Corresponding author. Pyzhevskiy 3, Moscow 119 017, Russia.
E-mail address: sitnov@ifaran.ru (S.A. Sitnov).

instability and overturning of Rossby waves (Pelly and Hoskins, 2003; Lupo et al., 2012).

Summer blocking episodes are accompanied by heat waves, lack of rainfall, drought, and often with the wildfires (Mokhov, 2011). Anomalously hot and dry weather associated with the unusually persistent atmospheric block over European Russia (ER) during the summer of 2010 contributed to the development of severe wildfires and pyrogenic emission into the atmosphere of various combustion products (including toxic ones) that in aggregate with a heat wave adversely affected human health (Witte et al., 2011; van Donkelaar et al., 2011; Sitnov, 2011a; Huijnen et al., 2012). In the pre-fire period for the summer of 2010, a rise in regional surface temperature in ER resulted in an increase of the regional atmospheric abundance of formaldehyde formed in the atmosphere due to the oxidation of isoprene emitted by plants (Sitnov and Mokhov, 2017).

Changes in regional atmospheric composition during atmospheric blocking events can be conditioned also by the peculiarities of the regional atmospheric circulation associated with blocks (Peters et al., 1995). It was shown that during the omega-type atmospheric blocks over ER during the summer 1972 and 2010, the total column water vapor (TCWV) field was characterized by anomalous spatial distribution, with a water vapor (WV) excess over the northern part of ER and a deficiency over the southern part of ER (Sitnov and Mokhov, 2013). The anomalous TCWV spatial distributions were associated mainly with the advection of humid maritime air from Mediterranean and Atlantic into the poleward flank of the blocking anticyclone (Sitnov et al., 2014).

A deficit of total column ozone (TCO) was found repeatedly within the domain of anticyclone (including the block) (e.g. Petzold, 1999; Barriopedro et al., 2010). The TCO deficit within the domain of atmospheric block is explained generally by the advection of ozone-depleted tropical air poleward, and the uplift of the tropopause and ascending air motions (Koch et al., 2005; Orsolini and Nikulin, 2006). The photochemical mechanisms of ozone destruction are also discussed (Petzold, 1999; Barriopedro et al., 2010). Sitnov and Mokhov (2015) argued that the TCO decrease within the domain of the prolonged atmospheric block over ER during the summer of 2010 was conditioned by the strong decrease of ozone in the lower stratosphere caused by the poleward quasi-horizontal advection of ozone-depleted tropical air and tropopause uplift. They also hypothesized that the negative TCO anomalies during this blocking event could be in part the result of the photochemical ozone destruction in the lower stratosphere due WV advection into this region (Sitnov and Mokhov, 2016).

Atmospheric blocking events are accompanied often by deep non-stationary mid-latitude local minima of TCO, called ozone mini-holes (OMHs) (Barriopedro et al., 2010). The maximum frequency of OMHs in the NH is observed within the Euro-Atlantic sector (James, 1998; Orsolini and Nikulin, 2006), where atmospheric blocking events also occur frequently (Lupo and Smith, 1995; Wiedenmann et al., 2002). The average duration of OMH is about three days, but under blocking conditions the duration may be up to two weeks (James, 1998). Since TCO modulates the intensity of solar ultraviolet (UV) radiation reaching the Earth's surface, living things within the domain of atmospheric block can be exposed to hazardous doses of biologically active UV radiation (Stick et al., 2006).

The purpose of this paper is to analyze the similarities and differences in the spatial and temporal variations in ozone, WV and temperature associated with a relatively short spring atmospheric block and anomalously persistent summer event over ER in 2010. Since numerical models project a warmer climate, an increase in anomalously prolonged summer atmospheric blocking events over

ER may be expected (Mokhov et al., 2014). Another motivation for this study is to obtain a more complete knowledge of possible changes in the atmospheric composition under unusual weather regimes occurring over the most densely populated region of Russia.

2. Data

Profiles of ozone, WV, and temperature as well as the tropopause characteristics obtained by the Atmospheric InfraRed Sounder (AIRS) instrument during the period from 30 August 2002 to 31 December 2015 were utilized for this study. AIRS is a space-borne high-resolution spectrometer, which measures infrared (IR) radiation in 2378 channels within the wavelength range of 3.7–15.4 μm (Chahine et al., 2006). The scanning system provides 95% daily data coverage for the Earth's surface. The AIRS algorithm for profile retrieval also utilizes the measurements from a collocated microwave radiometer AMSU (Advanced Microwave Sounding Unit), having the spatial resolution of 45 km in nadir (Mo, 1996). It is believed that joint analysis of radiation measurements in the infrared and microwave bands allows AIRS/AMSU to retrieve physically reasonable profiles in cases with up to 80% cloud cover (Susskind et al., 2006). The AIRS instrument was designed to retrieve temperature profiles with an accuracy of 1 K in a 1 km layer, the WV profile below 100 hPa with the accuracy of 15% in a 2 km layer, the ozone profile with the accuracy of 20%, as well as retrieving TCWV and TCO with the accuracy of 5% (Pagano et al., 2010). The validation of the AIRS TCO version 5 (V5) data for May–September 2010 using high-precision ground-based TCO measurements by Brewer spectrophotometers, operated at world ozone observation network stations Kislovodsk (43.7° N, 42.7° E) and Obninsk (55.1° N, 36.6° E) revealed a good agreement between satellite and ground-based TCO measurements (Sitnov and Mokhov, 2016; see also supplementary materials). AIRS and AMSU are installed on board the Aqua satellite, launched 4 May 2002 in a near-polar sun-synchronous orbit at a height of 705 km and a rotational period of 98.8 min (Aumann et al., 2003).

The AIRS V6 level 3 standard products (L3) comprising daily averaged measurements on the ascending and descending branches of an orbit with the quality indicators 'best' and 'good' and binned into 1° × 1° (latitude × longitude) grid cells [Tian et al., 2013] were used here. Ozone and temperature profiles are represented by data on 24 pressure levels between 1000 hPa and 1 hPa. WV profiles are represented at 12 levels between 1000 and 100 hPa, however the 150 hPa and 100 hPa level data are considered unreliable. TCO and TCWV data are calculated by integrating ozone and WV profiles, respectively. Tropopause pressure (P_{trop}) is derived from the air temperature profile using thermal tropopause definition (WMO, 1957). AIRS data (V6, L3) were obtained using the Giovanni system through <http://giovanni.gsfc.nasa.gov> (Acker and Leptoukh, 2007).

The daily zonal and meridional wind components as well as geopotential heights from the National Centers for Environmental Prediction/National Center for Atmospheric Research (NCEP/NCAR) reanalysis were used to represent atmospheric dynamics (Kistler et al., 2001). The data are provided on 2.5° by 2.5° latitude-longitude grids and available on 17 mandatory levels from 1000 hPa to 10 hPa available at <http://www.esrl.noaa.gov/psd/data/reanalysis>. These data are of sufficient resolution for determining the important dynamics related to a large-scale phenomenon such as blocking as shown in many published studies (e.g. Lupo et al., 2012).

3. Methods

3.1. Ozone and WV anomaly calculations

It is expected that atmospheric blocking impacts on ozone and WV concentrations manifest themselves on the background of large-scale natural variability for these gases. Using anomalies reduces the impact of systematic errors of observations and the impact of strong seasonal variations in ozone and WV, thus allowing for the more reliable extraction of the effects due to atmospheric blocking.

Latitude-longitude anomaly distributions during blocking events were calculated as deviations from spatial distributions in atmospheric parameters during the maximum development period of the 2010 spring and summer blocks from the average spatial distributions for atmospheric parameters during the respective periods 2003–2015, excepting 2010 (see also Sitnov et al., 2014). The daily regional anomaly time-series were obtained as deviations from regionally averaged daily values for atmospheric parameters during 2010 corresponding to the same day for the long-term regionally averaged daily values and smoothed using a 31-day running mean operator. Pressure-latitude anomalies cross-sections during the summer 2010 block were calculated as the deviations from the pressure-latitude distributions of atmospheric parameters for the maximum development period of the summer 2010 block from the average altitude-latitude distributions of atmospheric parameters during the period 2003–2015, excepting 2010.

The analysis of ozone, WV, and temperature measurements obtained on the ascending branch of an orbit (daytime data) bore a close resemblance to those obtained on the descending one (nighttime data). Therefore, in this study daytime and nighttime data are processed together.

3.2. Diagnosing the atmospheric blocking episodes

Fig. 1a shows the results of the daily atmospheric blocking diagnostics within the sector 20°–70° E longitude for the April–September 2010 period. For the diagnosis of the blocking episodes, the 500-hPa geopotential height (H500) data were analyzed using the Tibaldi and Molteni (1990) criterion. For each day and for every 2.5° longitude, the northern (G_N) and southern (G_S) meridional gradients of H500 were calculated using:

$$G_N = \frac{H500(\phi_N) - H500(\phi_0)}{\phi_N - \phi_0},$$

$$G_S = \frac{H500(\phi_0) - H500(\phi_S)}{\phi_0 - \phi_S},$$

where $\phi_N = 80^\circ \text{ N} + \delta$, $\phi_0 = 60^\circ \text{ N} + \delta$, $\phi_S = 40^\circ \text{ N} + \delta$, $\delta = -5^\circ, 0^\circ, 5^\circ$. A given longitude is defined as “blocked” if the following conditions are satisfied for at least one value of δ :

$$G_S > 0,$$

$$G_N < -10 \text{ m per latitude degree.}$$

The atmospheric blocking definitions often includes additionally the condition that blocking persists for at least five days (Lupo and Smith, 1995). Additionally, a NH blocking anticyclone during its lifetime should occur poleward of 35° N and the ridge should have an amplitude of greater than 5° latitude (Lupo and Smith, 1995). In accordance with these criteria, there was only two atmospheric blocking episodes that occurred within the time and spatial domain

identified here. These were a spring episode (3–20 May) and a summer episode (22 June–14 August) (Fig. 1a). In both episodes, the block positions did not remain strictly stationary. During May, there was a gradual drift of the blocking anticyclone from east to west. The prolonged summer blocking anticyclone was characterized by more complex spatio-temporal dynamics, manifesting also an amplitude vacillation (Shakina and Ivanova, 2010). According to Lupo et al. (2012), these blocking events were more intense than a typical event for their season and region using the Wiedenmann et al. (2002) block intensity diagnostic. In order to analyze the peculiarities of the TCO and TCWV fields associated with the 2010 spring and summer blocks, the 10-day periods 8–17 May and 1–10 August were selected for study. During these periods the blocking anticyclones intensified, therefore one can expect a clearer association between atmospheric chemical composition and atmospheric dynamics.

4. Results and discussion

4.1. Spatial distributions of TCO and TCWV under atmospheric blocking conditions

The mean spatial distributions of H500 during the periods 8–17 May 2010 (Fig. 1b) and 1–10 August 2010 (Fig. 1c) reveal a pattern characteristic of an omega-block, with the high-pressure area located over ER and two low-pressure areas over the adjacent regions. In the free troposphere the atmospheric circulation promoted the transport of air poleward within the longitudinal sector 10°–40° E and equatorward for the longitudinal sector 60°–90° E. Along with the differences for the absolute values of H500 of spring and summer, and in association with the seasonal cycles of tropospheric temperature and pressure, the blocking anticyclone center for 8–17 May 2010 was 15° longitude to the east relative to that of 1–10 August 2010 (Fig. 1b vs c). The May event also expressed a strong tilt in the ridge axis from SE to NW (Fig. 1b), as opposed to a weaker SW to NE ridge tilt during summer event (Fig. 1c). Within the domains of these blocking anticyclones, the spatial distributions of temperature anomalies are characterized by positive anomalies in the troposphere and by negative anomalies in the lower stratosphere (see supplementary materials).

The spatial distributions of the TCO anomalies (ΔTCO) during the spring (Fig. 1d) and summer (Fig. 1e) atmospheric blocking events reveal negative TCO anomalies over the poleward periphery of the spring block (when diagnosing block using the 500 hPa heights) and over the poleward and western peripheries of the summer block. Thus, the summer negative TCO anomalies encompass a much more extensive area. Overall, the magnitudes of TCO anomalies are not large, compared with the values generally adopted for OMHs definition (70 Dobson units (DU) or more (James, 1998)). The minimum value in the $1^\circ \times 1^\circ$ grid boxes (-33 DU or -10% in relation to the corresponding long-term mean) is observed during the summer block (Fig. 1e). Over the regions up and downstream from the blocking anticyclones, considerable positive TCO anomalies are revealed, reaching the values of 80 DU (+22%) during the spring block and 49 DU (+15%) during the summer event.

In contrast with ΔTCO , the spatial distributions of TCWV anomalies (ΔTCWV) are characterized by strong positive anomalies over the northern peripheries of the blocking anticyclones, reaching 10 kg m^{-2} (88%) in spring (Fig. 1f) and 11 kg m^{-2} (54%) in summer (Fig. 1g). These positive ΔTCWV anomalies are accompanied by weaker negative anomalies (-3 to -4 kg m^{-2} , about 30%) for the regions upstream and downstream. The larger percentage value of the spring WV anomaly can be explained by the seasonal variability of WV over ER, which reaches a maximum in summer

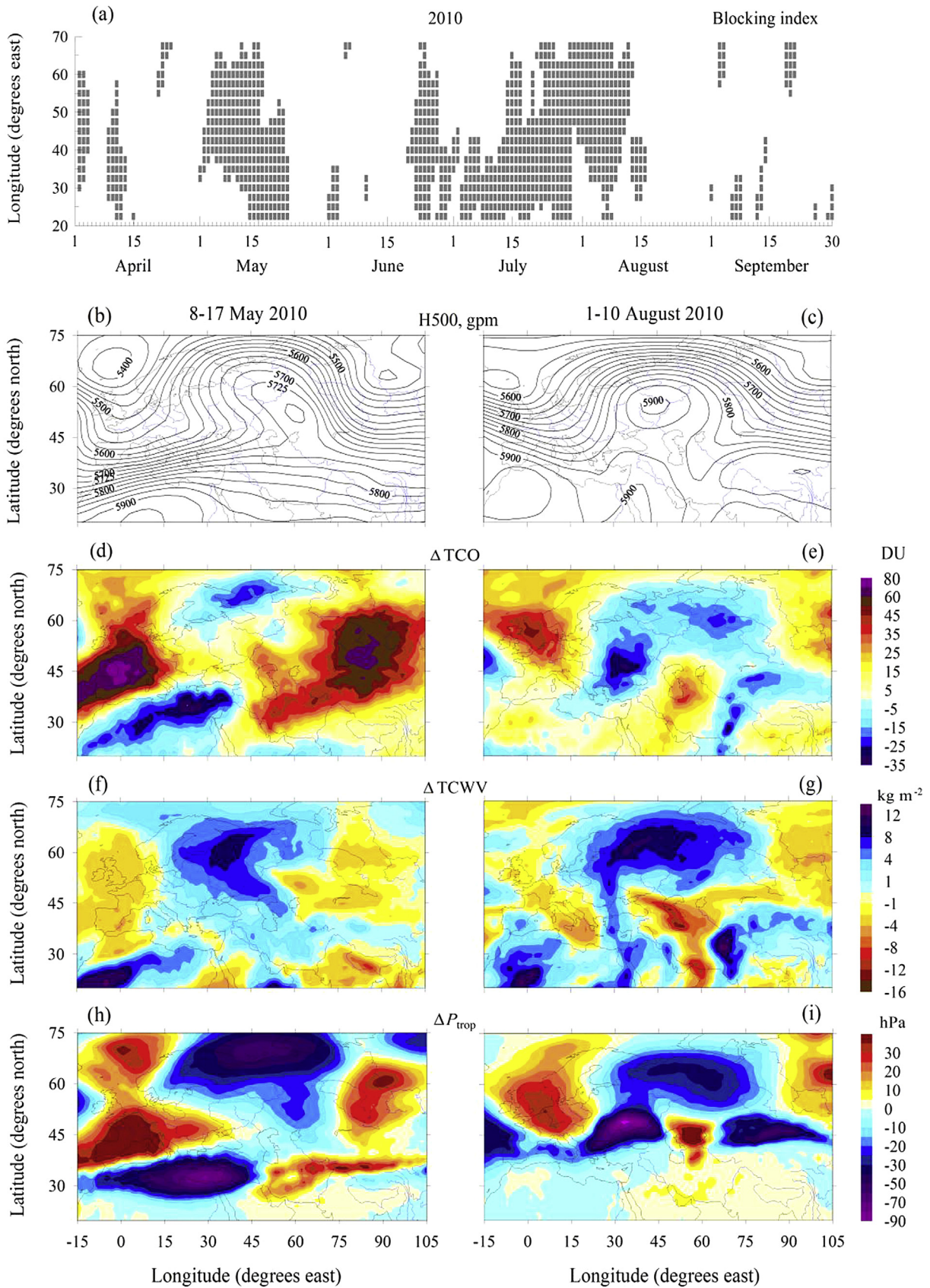


Fig. 1. (a) Longitudes (left axis) and days (lower axis) of atmospheric blocking according to the blocking criteria of [Tibaldi and Molteni \(1990\)](#) (shaded) in the April–September period of 2010, (b, c) Spatial distributions in 500-hPa geopotential heights and spatial distributions of the mean anomalies in: (d, e) TCO (color: -35 to 50 Dobson units (DU) with increments of 5 DU, 50 to 80 DU with increments of 10 DU), (f, g) TCWV (color: -12 to 12 kg m^{-2} with increments of 2 kg m^{-2} , ± 1 , -14 and -16 kg m^{-2}), and (h, i) P_{trop} (color: -90 to -30 with increments of 10 hPa, -30 to 35 hPa with increments of 5 hPa), during the periods of 8–17 May 2010 (left side) and 1–10 August 2010 (right side).

(Sitnov, 2011b). The spatial distribution of TCWV anomalies during the first ten days of August 2010 (Fig. 1g) is in accord with that of precipitable WV anomalies obtained by Sitnov et al. (2014) using MODIS data.

During both the spring and summer blocking episodes a negative correlation between spatial TCO and TCWV anomalies is found (cf. Fig. 1d with Fig. 1f and e with Fig. 1g) with some strengthening of the correlation over the poleward region. The spatial correlation coefficients between ΔTCO and ΔTCWV for the periods 8–17 May and 1–10 August 2010, calculated over the region bounded by the ER coordinates defined in Fig. 1 (20° – 75° N and 15° W– 105° E) are 0.48 (the 95% confidence intervals: -0.50 , -0.46) and -0.50 (-0.52 , -0.48). The correlations calculated over the territory poleward of 45° N reach values -0.71 (-0.73 , -0.69) and -0.65 (-0.67 , -0.63), respectively. As much as 90% of the ozone is in the stratosphere, but almost all WV is in the lowest 2-km of the atmosphere (Perov and Khrgian, 1980), thus the close relationship between ΔTCO and ΔTCWV seems rather unexpected and poorly documented. Nevertheless, the relationship can be explained qualitatively by dynamic factors. Climatologically, the TCO increases with latitude, TCWV on the contrary decreases from equator to pole, and the meridional advections likely promote the negative correlation between ΔTCO and ΔTCWV . Lastly, the ΔP_{trop} anomalies (Fig. 1h, i) were stronger for the spring blocking episode, which was more intense than the summer season event.

Statistical significance of the ΔTCO and ΔTCWV anomalies, and ΔP_{trop} was calculated for each of the $1^{\circ} \times 1^{\circ}$ grid cell using the two-sample Welch's *t*-test, which is more reliable than Student's *t*-test when two samples have unequal sample sizes and unequal variances (Fig. 2). The results indicate that within the domains of the spring and summer 2010 atmospheric blocks, the positive anomalies of WV and negative anomalies of the P_{trop} are significant ($\alpha = 0.05$) (cf. Fig. 1f with Fig. 2c, Fig. 1g with Fig. 2d, Fig. 1h with Figs. 2e, 1i and 2f). When comparing Fig. 2 with Fig. 1, it can be seen that within the domains upstream and downstream to the blocks, the negative WV anomalies as well as positive ozone - and P_{trop} anomalies are also statistically significant. At the same time the negative TCO anomalies within the domains of the blocks are at the limits of the standard levels of statistical significance. However it should be noted that the estimation of significance thresholds relates to the significance of anomalies in the spatial resolution $1^{\circ} \times 1^{\circ}$. When assessing the reliability of the existence of a conglomerate of the anomalies of the same sign, the requirement for the statistical significance of each individual anomaly seems unnecessarily strict.

The presence of meridional transports over a wide range of height levels during the spring and summer 2010 atmospheric blocks is illustrated in Fig. 3. Comparing the spatial distributions of ΔTCWV and the 700-hPa wind field indicates a close association between the spatial inhomogeneities in ΔTCWV with the atmospheric circulation in the free troposphere (cf. Fig. 1f with Fig. 3i and Fig. 1g with Fig. 3j). In particular, the spatial distribution of ΔTCWV 8–17 May 2010 (Fig. 1f) reflects air mass transport from SE to NW due to the tilt of the ridge's western flank (Fig. 1b). The surplus of TCWV over the domain of blocking anticyclone can be explained by the advection of warm subtropical air, enriched by WV poleward of ER along the western periphery block center, while the deficit of TCWV over the areas conterminous with the anticyclone could be due to the advection of the WV depleted arctic air (Fig. 3e,g,i).

It was not expected that the spatial distributions of ΔTCO in both examined blocking episodes would bear little relation to the horizontal wind distribution in the stratosphere (Fig. 3a–f) (since the bulk of ozone is in the stratosphere). For example, positive TCO

anomalies over the regions west and east of the spring 2010 block are accompanied by the meridional flows having opposite directions at the 50-hPa level (cf. Fig. 1d and Fig. 3c) in spite of the fact that this level is near the maximum of the mid-latitude ozone profile (Perov and Khrgian, 1980). Comparative analysis of ozone anomalies with winds at different levels indicates that the TCO anomalies are associated, to a greater extent, with atmospheric circulations near the tropopause (cf. Fig. 1d with Fig. 3e,g and Fig. 1e with Fig. 3f,h). This distribution could be explained by a sharp wind maximum at this level, and, thus, is the dominant component of ozone fluxes in the tropopause region for the formation of TCO field. The negative TCO anomalies within the atmospheric blocking regions was explained further by the advection of subtropical air with low total ozone content poleward and following turning eastward due to the large-scale anticyclonic circulation (Fig. 3c–h and also Fig. 7a). The positive TCO anomalies over the adjacent regions may be the result of the equatorward advection of ozone-enriched arctic air.

An important mechanism for TCO changes is known to be associated with the changes in the tropopause position. Intra-seasonal changes in the tropopause are closely related to the vertical air motions in the upper troposphere - lower stratosphere (UTLS) (Petzold et al., 1994). Fig. 1h and f show P_{trop} anomalies (ΔP_{trop}) during the spring and summer atmospheric blocks, respectively, calculated similar to those of ΔTCO and ΔTCWV . The increase or decrease in ΔP_{trop} is associated with lowering or lifting of the tropopause, respectively. A comparison of Fig. 1d with Fig. 1h and e with Fig. 1i reveals close similarity between the spatial distributions of ΔTCO and ΔP_{trop} during both blocking episodes. The correlation coefficients between the ΔTCO and ΔP_{trop} spatial distributions within the region 20° – 75° N, 15° W– 105° E during the periods 8–17 May 2010 and 1–10 August 2010 are 0.75 (0.74, 0.76) and 0.77 (0.76, 0.78), respectively. The link between ΔTCWV and ΔP_{trop} is much weaker. The spatial correlation coefficients between ΔTCWV and ΔP_{trop} for the respective periods are -0.38 (-0.40 , -0.36) and -0.30 (-0.32 , -0.28). Positive correlations between ΔTCO and ΔP_{trop} in the block region can be partially explained by the advection of air masses originating from subtropical latitudes with low TCO and high tropopause, and also by the advection of arctic air, with increased TCO and a lower tropopause (cf. Fig. 1d with Fig. 3c, e, g and Fig. 1e with Fig. 3d, f, h). However, some details of the ΔTCO distributions are difficult to explain by quasi-horizontal advection.

Local TCO anomalies (especially the anomaly centered near 45° N, 30° E during the period of 1–10 August 2010 (Fig. 1e)) are difficult to explain by horizontal motions. Rather, they could be associated with the vertical motions of air. Ascending air in the UTLS results in the replacement of air from the lower stratosphere characterized by relatively high ozone mixing ratio with the air from the upper troposphere possessing relatively low mixing ratio of ozone. Additionally, since the ozone relaxation time decreases with height, the ozone concentration in the upper part of the profile finds photochemical equilibrium faster than the lower part. Therefore, in the presence of overall upward vertical motion extending through a deep atmospheric layer should result in a decrease for total columnar ozone content (Perov and Khrgian, 1980). On the other hand, rapid upward motion in the UTLS is associated with adiabatic cooling and, consequently, a decrease in temperature and tropopause (decrease in P_{trop}). Conversely, subsidence occurring in a deep layer leads a depression in tropopause height (increase in P_{trop}) and an increase in TCO. Relatively low correlation coefficients between ΔTCWV and ΔP_{trop} are probably indicative of a relatively weak contribution of the vertical motions

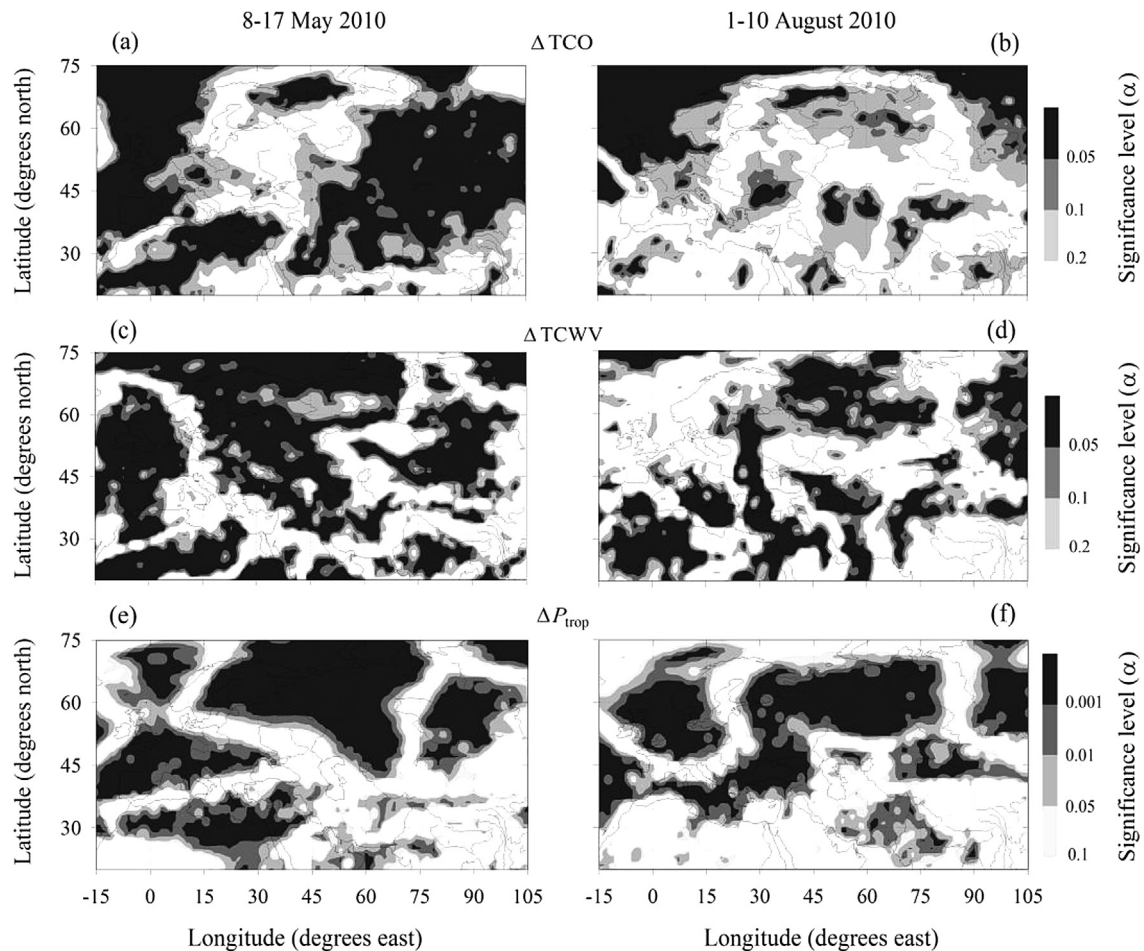


Fig. 2. (a) The levels of significance of individual ($1^\circ \times 1^\circ$) anomalies in TCO (a,b), TCWV (c,d), and P_{trop} (e,f) in the periods 8–17 May 2010 (left side) and 1–10 August 2010 (right side).

to the TCWV field formation, compared to their contribution to the TCO field formation. Apparently, the anomalies of TCWV during the spring and summer atmospheric blocking events in 2010 are associated with the horizontal advection of WV to a greater degree.

The spatial structure of the vertical wind velocities which occurred in the middle troposphere during the maximum strengthening phase for the summer blocking anticyclone over ER in 2010 were presented by Sitnov et al. (2014). The results of this earlier work show the presence of ascending air motions over the western and northern flanks of the blocking anticyclone with the velocities of $1\text{--}1.5 \text{ cm s}^{-1}$. A general overview of the vertical motions during the spring and summer atmospheric blocking events over ER in 2010 can be also inferred from the calculation of horizontal divergence in the mean wind field (during the 10-day intervals) at several pressure levels (Fig. 3). The results show that poleward of 45° N , over the western (eastern) flank of the blocking regions, poleward (equatorward) air flow is accompanied by divergence (convergence) of horizontal wind, respectively. The absolute values of the horizontal divergence ($\text{div}_h \mathbf{V}$) increase with height in the troposphere and decrease with height in the stratosphere peaking just above the tropopause. Thus in the UTLS over the western (eastern) flanks of the blocks, ascending (descending) motions of air should occur, respectively. The patterns of vertical motions are rather crude since these were calculated using the divergence in horizontal wind fields averaged over the 10-day periods.

It is believed that atmospheric blocking events are closely related to the dynamics of planetary Rossby waves (Pelly and Hoskins, 2003). The global distributions of TCO, TCWV, and P_{trop} anomalies during the summer 2010 atmospheric blocking event reveal clearly the large-scale wave structures (Fig. 4). It can be seen that in the middle latitudes, the field of horizontal wind reveals jet maxima or streaks generally flowing from west to east. (Fig. 4d). A Rossby wave train (RWT) originates in the region of the Hawaiian archipelago (21° N , 151° W) over the Pacific Ocean. The amplitude of RWT increases from west to east reaching a maximum within the domain of the atmospheric block over ER. Note that ridges and troughs are associated with negative and positive anomalies in TCO, respectively (cf. Fig. 4d with Fig. 4a). It has been shown earlier that for planetary waves embedded in zonal flow, a poleward (equatorward) shift of the flow is always accompanied by an ascent (descent) of air, respectively (Matsuno, 1980). A numerical simulation of the ozone transport by planetary waves showed that the maximum increase (decrease) in TCO should occur in the trough (ridge) of the wave, respectively (Bekoryukov, 1965). It can be seen that the global distribution of TCO anomalies during the summer 2010 ER atmospheric blocking is consistent with the results of the latter study (cf. Fig. 4a and d).

The wave-like structure of ΔTCWV is less clear than that of the TCO anomalies (Fig. 4b). In the mid-latitudes, however, TCWV anomalies associated with RWT negatively correlated with TCO. Unlike TCO, the magnitudes of the TCWV anomalies are greater in

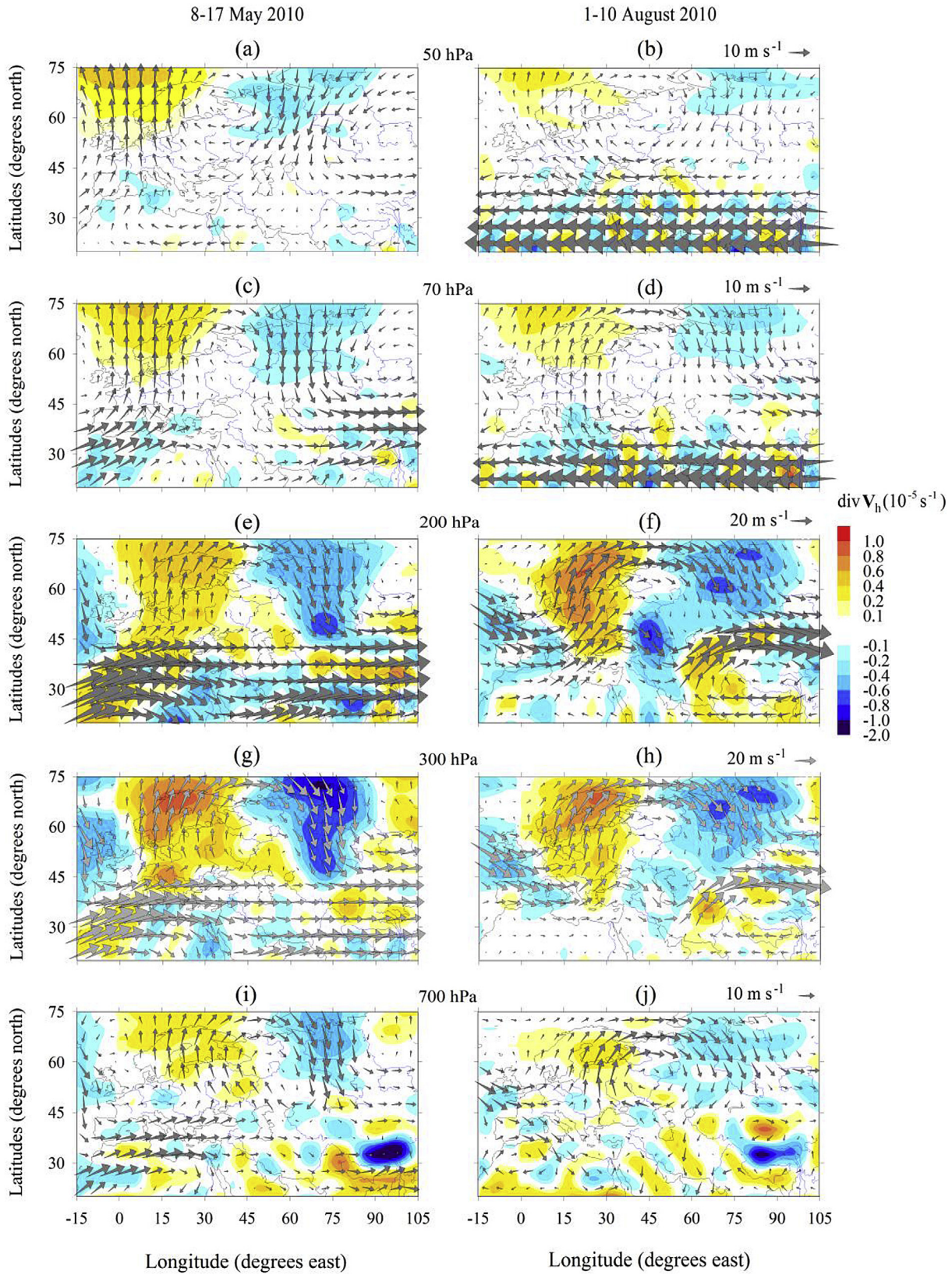


Fig. 3. Spatial distributions of the mean horizontal wind vectors (arrows) and horizontal divergence of the wind (color scale) at the levels: (a, b) 50 hPa, (c, d) 70 hPa, (e, f) 200 hPa, (g, h) 300 hPa, and (i, j) 700 hPa in the period 8–17 May 2010 (left side) and 1–10 August 2010 (right side).

ridges, but weaker in troughs. The wave-pattern of anomalies is revealed also on the P_{trop} (Fig. 4c). The spatial distribution of

negative P_{trop} anomalies nearly coincides with the axis of the jet stream (Fig. 4d) while the negative anomaly associated with the

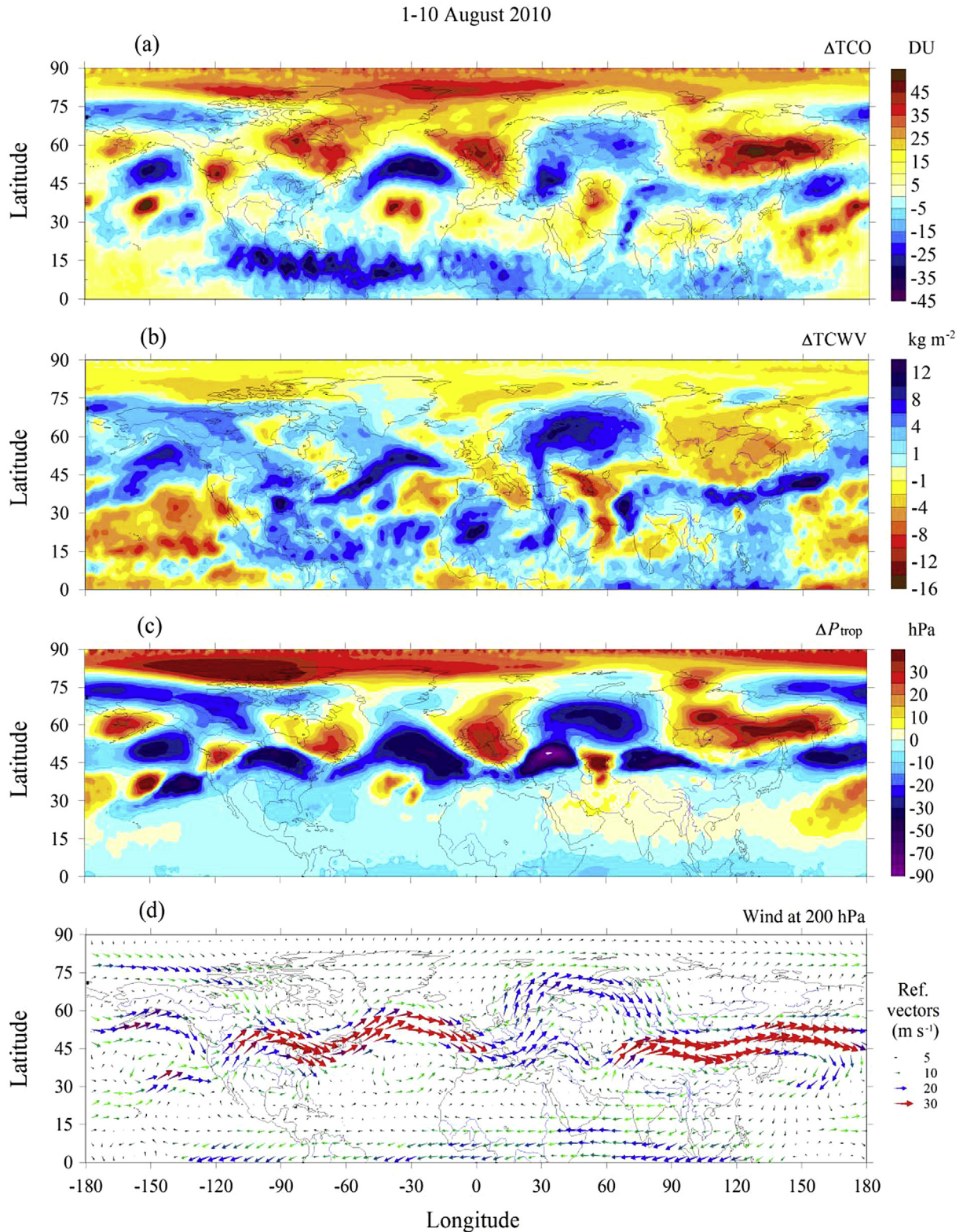


Fig. 4. Spatial distributions in the Northern Hemisphere of the mean anomalies in: (a) TCO, (b) TCWV, and (c) P_{trop} , and (d) the mean wind vectors at 200-hPa level in the period 1–10 August 2010.

block is represented by split flow (Fig. 4d). In the troughs, (poleward of the jet axis) weaker positive ΔP_{trop} anomalies are observed. In the latitude belt 30° – 75° N, ΔP_{trop} is highly correlated with ΔTCO . The spatial correlation between ΔP_{trop} and ΔTCO reached

0.83 (0.82–0.84). Positive TCO anomalies are also observed within regions of persistent and closed cyclonic circulations, in particular, those centered at (37° N, 152° W) and (32° N, 38° W). The planetary wave structure is less pronounced during the spring blocking event

(see supplementary materials).

4.2. Temporal evolution of TCO and TCWV, and dynamical parameters within the 2010 ER atmospheric blocking events

When examining the spatial distribution and magnitude of TCO and TCWV anomalies during the spring and summer 2010

atmospheric blocking events, Fig. 1d–g does not elucidate the time evolution of these anomalies. Fig. 5 shows the temporal changes of sub-regional mean daily.

TCO, TCWV, and P_{trop} anomalies, and the accompanying variations for the regional mean tropopause and stratospheric region meridional and zonal winds. Fig. 5 depicts the winds and not their anomalies, since the former provides information about the

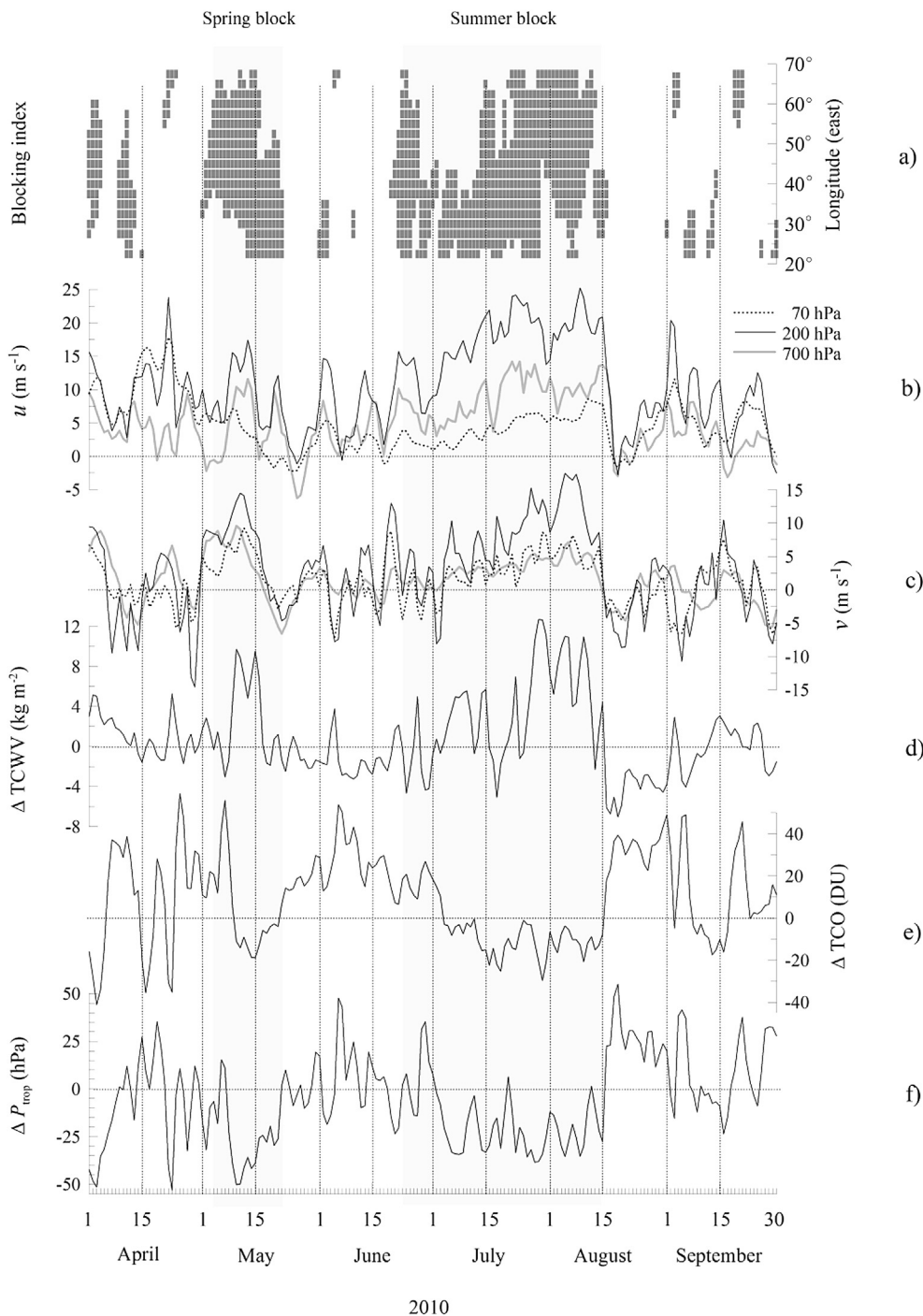


Fig. 5. (a) Longitudes (right axis) and days (lower axis) of atmospheric blocking according to the blocking criteria of Tibaldi and Molteni (1990) (shaded), (b) daily mean zonal wind, averaged over the region 65°–75° N, 30°–60° E at the levels of 700 hPa (thick grey line), 200 hPa (thin black line), and 70 hPa (dashed line), (c) daily mean meridional wind, averaged over the region 45°–75° N, 15°–30° E at the same levels, and averaged over the region 60°–70° N, 30°–60° E daily anomalies in: (d) TCWV, (e) TCO, and (f) P_{trop} in April–September 2010. The regionally averaged daily anomalies were calculated as deviations of the regionally averaged daily values of atmospheric parameters in 2010 from corresponding to this day the long-term regionally averaged daily values, based on data from 1 September 2002 to 30 September 2015 (excluding 2010), smoothed by the 31-day running mean operator.

direction of air transport. Variations in u , v and ΔP_{trop} demonstrate the basic physical mechanisms for changes in TCO and TCWV within the northern ER during block development, namely the horizontal advection of air and the changes in the tropopause position. It is known that the intraseasonal variations in P_{trop} are closely related to atmospheric dynamics, in particular, the vertical motions in the UTLS region (Petzold et al., 1994; Petzold, 1999).

Both the spring and summer blocking episodes were accompanied over the northern part of ER by negative TCO anomalies and positive TCWV anomalies (cf. Fig. 5a with Fig. 5e and d). Unlike the spring episode, the summer one is characterized by a rather prolonged development stage for TCO and TCWV (and also P_{trop}) anomalies and by a rapid change in the sign of the anomalies during block decay. This corresponded to the evolution of the planetary-scale dynamics for this event shown in Lupu et al. (2012). Interestingly, TCO and P_{trop} over the northern ER began to decrease even before the formation of the summer block (as it diagnosed using H500) (cf. Fig. 5a with Fig. 5e). The gradual development of TCO, TCWV and P_{trop} anomalies was accompanied by the gradual strengthening of u and v (Fig. 5b and c). These anomalies were associated with the development of the summer blocking anticyclone over ER, and reached its culmination during the first ten days of August 2010. However, as expected the maximum values of u and v were observed at 200 hPa during both blocking events. This was slightly above the position of the mid-latitude tropopause, where the atmospheric circulation was also closely related with Rossby wave dynamics (see also Fig. 4d). Fig. 5b and c also show that the sharp decrease of the wind components during the summer block decay period was accompanied by similar abrupt changes in ΔTCO , ΔTCWV and ΔP_{trop} . The rapid changes in all examined atmospheric parameters near the termination of the summer blocking event were apparently associated with replacement of the strong stationary anticyclone by the upper-level cyclone that persisted over the Polar Ural during the second half of August 2010 (see supplementary materials). After the summer block termination, the TCO, TCWV and P_{trop} anomalies with the opposite signs of those during atmospheric blocking persisted over the northern ER for two weeks (Fig. 5).

Quantitative relationships between the analyzed atmospheric parameters are shown in Table 1, which contains a correlation matrix of ΔTCO , ΔTCWV , ΔP_{trop} , u and v , calculated for the period April–September 2010 and separately for atmospheric blocking conditions. The latter are diagnosed at 45° E, which is close to the block center and midway between 30° E and 60° E (see also Fig. 5a). It can be seen in Table 1 that high correlations between the tracer variables and meteorological parameters manifest themselves between the ΔTCO and ΔP_{trop} during both the periods (0.73). Also, high correlations were found for the full period between ΔTCWV and ΔP_{trop} (–0.72). Moderately high correlations were found

between ΔTCO and ΔTCWV when calculated over the full period (–0.61).

The data in Table 1 show a closer correlation between ΔTCO and ΔTCWV with the wind at 200 hPa than with the winds at the 700 or 70 hPa levels. This indicates the important (possibly leading) role of atmospheric dynamics near the tropopause in the formation of the TCO and TCWV fields during the spring and summer 2010 atmospheric blocking events. In turn, the variations of the wind at 200 hPa more closely correlate with variations of wind in the troposphere than with those in the stratosphere. This is indicative of the link between the blocking anticyclone in the troposphere, and the stationary Rossby wave ridge in the tropopause region. Somewhat unexpectedly, correlation coefficients during blocking conditions are generally lower than those during the whole period even though the reverse was expected (Pelly and Hoskins, 2003). This may be explained by the strong and concomitant changes in all the atmospheric parameters observed at the termination of the summer 2010 block and during the following ten-day period. These changes in flow regime may have contributed substantially to the correlation, but revealed themselves only after blocking termination.

4.3. Vertical structures of the ozone, WV and temperature anomalies

4.3.1. Anomaly pressure-time cross sections

Analysis of the TCO and TCWV previously provided some information about the pressure levels where changes of ozone and WV occurred. Fig. 6 shows the vertical structures of the anomalies in the volume mixing ratios (VMRs) of ozone (ΔO_3) and WV ($\Delta\text{H}_2\text{O}$) as well as the air temperature anomalies (ΔT) in more detail.

A characteristic feature of the altitude-time evolution in stratospheric ozone under blocking conditions is the presence of ozone anomalies of different signs, simultaneously existing at different altitudes, which obviously leads to their mutual compensation in TCO (Fig. 6a). This fact explains the weak manifestation of negative TCO anomalies over the northern ER during the spring block (see also Fig. 1d). At the same time ozone anomalies tend to have the same signs in the lower stratosphere and in the troposphere. The negative ozone anomalies in the lower stratosphere and troposphere during the summer block were more widespread, persistent, and higher in height however, than those associated with the spring event.

During both the spring and summer 2010 blocking events the positive WV anomalies in the lower troposphere reached values of 3.5 and 6 ($\times 10^{-3}$), respectively (Fig. 6c). It is demonstrated here that the anomalies spanned not only the entire troposphere, but also penetrated in the lower stratosphere. At the 200 hPa level, the increase in WV during the periods 8–17 May 2010 and 1–10 August

Table 1

Correlation matrix for the daily TCO, TCWV, and P_{trop} anomalies averaged over the region 60°–70° N, 30°–60° E, the mean meridional wind (v) over Central Europe (45°–75° N, 15°–30° E), as well as the mean zonal wind (u) over northern European Russia (65°–75° N, 30°–60° E) at the pressure levels 700, 200, and 70 hPa. Correlations above the diagonal are obtained in the period April–September 2010, while those below the diagonal - under atmospheric blocking conditions, when the block is diagnosed at 45° E. Correlation coefficients, exceeding 0.6 are shown in bold text. Values showing no correlation significant at the 0.95 confidence level are shaded.

	ΔTCO	ΔTCWV	ΔP_{trop}	v_{700}	v_{200}	v_{70}	u_{700}	u_{200}	u_{70}
ΔTCO	1.00	–0.61	0.73	–0.50	–0.53	–0.32	–0.47	–0.64	–0.25
ΔTCWV	–0.45	1.00	–0.72	0.50	0.56	0.54	0.41	0.54	0.23
ΔP_{trop}	0.73	–0.56	1.00	–0.59	–0.62	–0.57	–0.48	–0.63	–0.15
v_{700}	–0.36	0.45	–0.50	1.00	0.85	0.56	0.34	0.40	–0.01
v_{200}	–0.40	0.54	–0.52	0.85	1.00	0.74	0.42	0.56	0.09
v_{70}	–0.19	0.40	–0.37	0.66	0.74	1.00	0.29	0.46	0.31
u_{700}	–0.52	0.36	–0.36	0.25	0.38	0.04	1.00	0.82	0.24
u_{200}	–0.54	0.36	–0.35	0.32	0.53	0.20	0.84	1.00	0.42
u_{70}	–0.17	0.31	–0.20	0.38	0.38	0.64	0.11	0.25	1.00

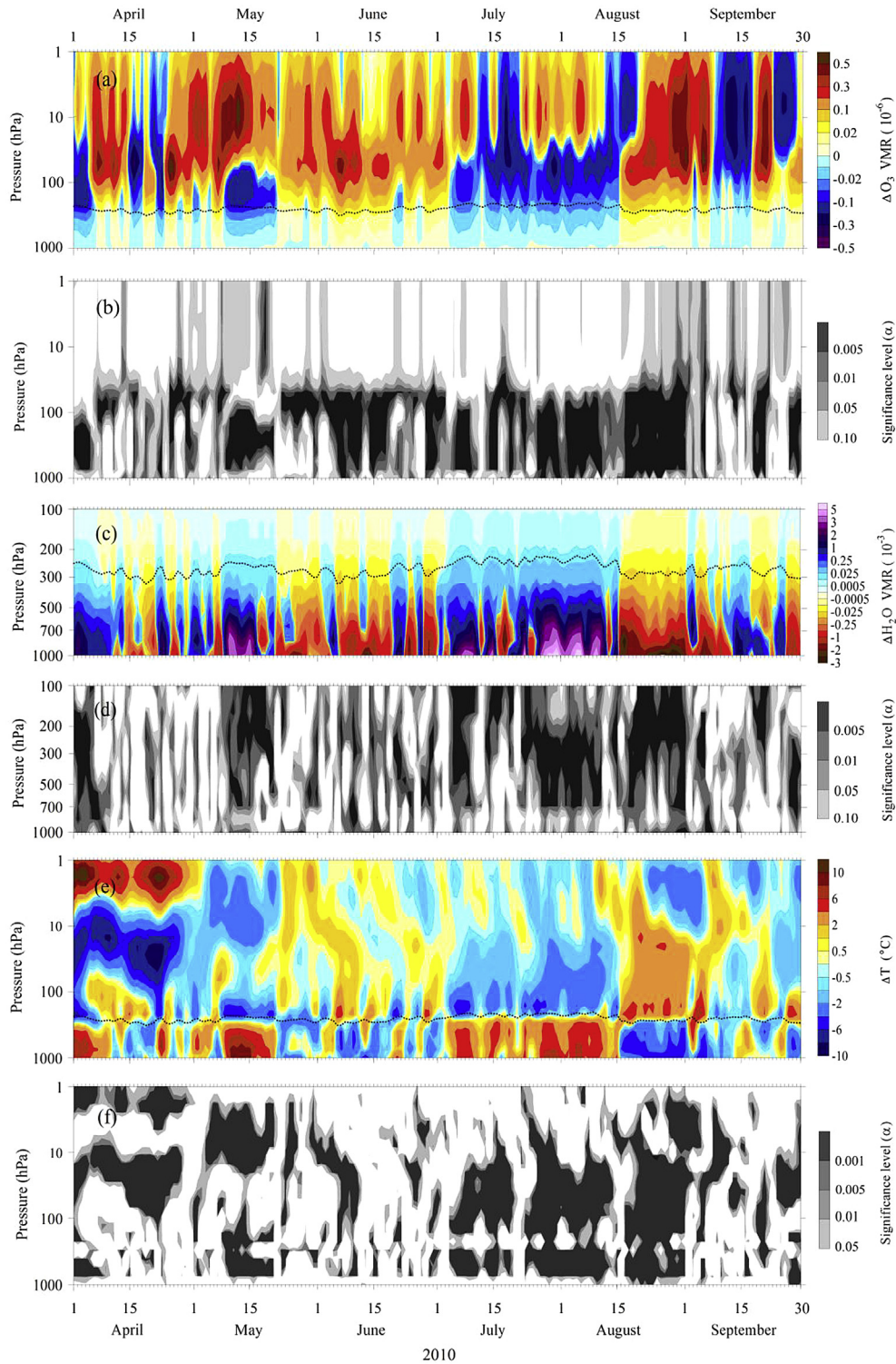


Fig. 6. Pressure-time distributions of the regionally mean daily anomalies in: (a) ozone (ΔO_3), (c) WV (ΔH_2O), and (e) temperature (ΔT), averaged over the region 60° – 70° N, 30° – 60° E in April–September 2010; (b, d, f) - the levels of significance of the anomalies in ozone, WV, and temperature (respectively) calculated for individual days and levels. Dashed lines depict daily position of the regionally mean tropopause position.

2010 reached 0.0032×10^{-3} (3.2 ppm or 39% relative to the corresponding long-term mean) and 0.0066×10^{-3} (6.6 ppm or 43%, respectively) (Fig. 6c). Additionally, during both the spring and summer atmospheric blocking events, a noticeable increase in tropopause height was observed.

A prominent feature in the altitude-time cross-section of

temperature changes is the thermal anomalies of opposite signs, which manifest themselves in the troposphere and lower stratosphere (Fig. 6e). The changes in sign of the anomalies occur at tropopause level. Dipole-like structure for the temperature anomalies is seen clearly during both atmospheric blocking events. During these periods the positive tropospheric temperature

anomalies (reaching the surface layer the values of +10 °C for spring and +7.5 °C for summer) are accompanied by negative temperature anomalies in the lower stratosphere (−5.5 °C). It is also shown that following the end of the summer blocking period, the signs of the tropospheric and stratospheric thermal anomalies reversed and persisted until the end of August.

The statistical significance of the anomalies in the ozone, WV, and temperature profiles was calculated for each day and level using the two-sample Welch’s *t*-test (Fig. 6b,d,f). It can be seen that during spring and summer atmospheric blocking events the negative ozone anomalies and positive WV anomalies manifesting in the troposphere and lower stratosphere over the northern ER are statistically significant. Comparison Fig. 6f with Fig. 6e also confirms the reality of dipole-like altitude structures in temperature anomalies observed over this region, with the positive temperature anomalies in the troposphere and negative ones in the lower stratosphere.

4.3.2. Pressure-latitude cross sections of the anomalies

Since the meridional advection plays a crucial role in the formation of TCO and TCWV anomalies within the domains of atmospheric omega-blocks, an analysis of the latitudinal distributions of atmospheric parameters during these events is of great interest. Fig. 7 shows the pressure-latitude distribution of ozone, WV and

temperature anomalies over the western periphery of the summer blocking high (see also Fig. 1c, e, g).

A characteristic feature of the altitude-latitude distribution of the ozone anomalies is the columnar structure and the alternating of the anomalies’ signs from the equator to the pole (Fig. 7a). Over the subtropical- and polar latitudes, there are positive ozone anomalies at all levels, while over the middle latitudes the negative ozone anomalies dominate in the lower stratosphere and troposphere. The negative anomalies reach extreme values in the lower stratosphere over the latitudes centered at 45° N (up to −0.4 ppm). It can be seen that at these latitudes an abrupt change in the tropopause position occurred.

The pressure-latitude distribution of WV anomalies (Fig. 7c) during the 1–10 August 2010 period is characterized by an extended region of positive WV anomalies in the troposphere stretching from 7° N to 74° N latitude (see also Fig. 1d). The maximum WV anomalies reached $3.65 (\times 10^{-3})$ in the surface layer at 60° N. Within the latitudes 47°–74° N positive WV anomalies covered the entire troposphere and penetrated into the lower stratosphere. In the middle latitudes the surplus of WV in the stratosphere is observed immediately after the lowering of the tropopause position (from the tropical-to polar tropopause).

Contrary with ozone, the main feature in the pressure-latitude distribution of temperature anomalies (Fig. 7e) is the alternating

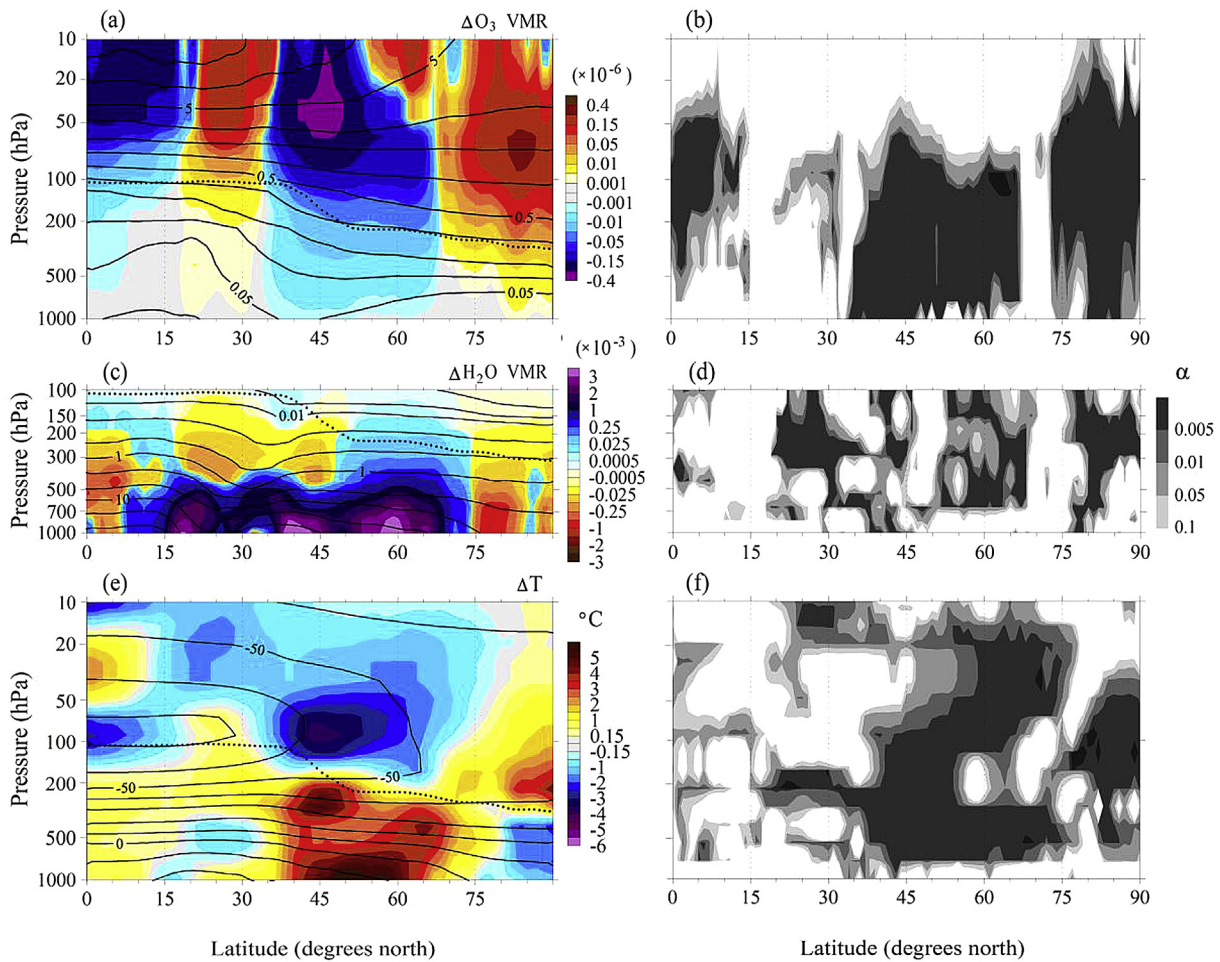


Fig. 7. Pressure-latitude distributions of the anomalies in: (a) ozone (ΔO_3), (c) WV (ΔH_2O), and (e) temperature (ΔT), averaged in the longitudinal sector 25°–35° E during 1–10 August 2010 (color scales) and the corresponding long-term distributions in the periods 1–10 August 2003–2015 (excluding 2010) of (a) ozone (isolines: 0.03, 0.05, 0.075, 0.125, 0.25, 0.5, 1, 2, 3, 5, 7, 9 ppm), (c) WV (isolines: 0.003, 0.005, 0.01, 0.05, 0.25, 1, 3, 6, 10, 15, 20 ($\times 10^{-3}$)), and (e) temperature (isolines, step 10 °C). Dashed lines depict the tropopause position in 1–10 August 2010. The levels of significance of the anomalies in ozone (b), WV (d), and temperature (f) calculated for the anomalies at individual latitudes and levels.

signs of these anomalies with altitude. The dipole-like structure of the temperature anomalies reveals itself most noticeably over the middle latitudes, where strong tropospheric positive anomalies, reaching $+6.5\text{ }^{\circ}\text{C}$ near the surface layer are accompanied by negative stratospheric anomalies of $-3.8\text{ }^{\circ}\text{C}$ slightly above the tropopause.

Note the proximity of the temperature anomaly dipole structure and that of negative ozone anomalies in the mid-latitudes, which is a result of the presence of the blocking events. Since the climatological meridional temperature gradients in the extratropical troposphere and stratosphere are characterized by opposite signs (see isolines in Fig. 7e), the meridional air motions spanning nearly the depth of the column can be a cause or manifestation of the temperature anomalies of the opposite signs in the troposphere and lower stratosphere. The dipole-like structure of weaker temperature anomalies, which are of opposite sign to those in the mid-latitudes, is observed also north of 80° N .

The statistical significance of ozone, WV and temperature anomaly profiles was calculated for individual anomalies at each latitude and level (Fig. 7b,d,f). It can be seen that over the middle- and high latitudes, the vertical anomaly structures described above are statistically significant.

Latitudinal cross-sections of the meridional and zonal wind profiles over the western periphery of the summer block are shown in Fig. 8. It can be seen that southerly winds prevail in the mid-latitude troposphere and lower stratosphere, whose speed increases with height reaching the maximum 17 m s^{-1} at the 250 hPa level over 65° N . In particular close to the tropopause break, the southerly winds with speeds exceeding 10 m s^{-1} are observed. In the mid-latitude troposphere and lower stratosphere, westerly winds prevail reaching the maxima over 45° N in the vicinity of the tropopause break and over 70° N in the tropopause layer, reflecting the jet position and split flow that is typical for the omega-type blocking (e.g. Rex, 1950) (see also Fig. 3f). Easterly winds dominate tropical atmosphere, reaching the speeds of $25\text{--}30\text{ m s}^{-1}$ in the middle stratosphere over the equator. With an increase in latitude, the extent of the westerlies expands from the surface on up, while the region occupied by the easterlies narrows.

In early August, within the longitudinal sector $25^{\circ}\text{--}35^{\circ}\text{ E}$, the long-term distribution of ozone mixing ratio in the UTLS increases

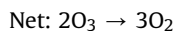
from equator to pole (Fig. 7a). Therefore the poleward transport of air masses over the western periphery of the summer blocking anticyclone contributed to inflow of the ozone-depleted air into the domain of atmospheric blocking (Fig. 8) thus reducing ozone over the blocked region. The poleward advection favors also the inflow of WV-enriched subtropical air into the blocked region (cf. Fig. 7c with Fig. 8). It can be seen that through the tropopause break the moist subtropical air could penetrate directly from the low-latitude upper troposphere in the mid-latitude lower stratosphere.

4.4. Photochemical destruction of ozone within the domain of atmospheric block

Another mechanism which may be responsible for negative correlation between ozone and WV may be photochemical destruction of ozone in reactions, involving WV (e.g. Hunt, 1966). As shown above, within the atmospheric blocking region there was an excess in WV both in the troposphere and in the lower stratosphere, which was accompanied by a concurrent deficit in ozone concentration (cf. Fig. 6a with Fig. 6c and also Fig. 7a with Fig. 7c). It is known that WV oxidation by atomic oxygen in the reaction



is an important source for hydroxyl radicals in the stratosphere. These radicals regulate the intensity of the hydrogen catalytic cycle for ozone destruction



The chain of the reactions in the hydrogen catalytic cycle terminates through the reaction

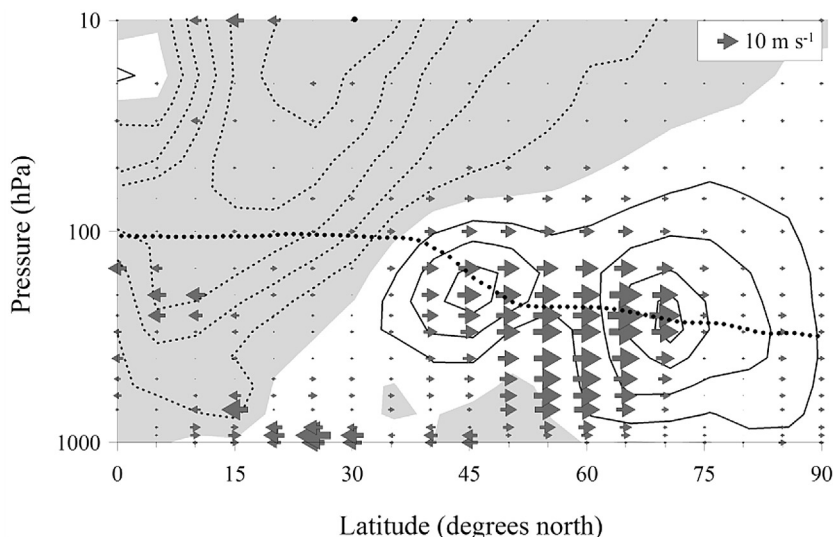


Fig. 8. Pressure-latitude cross-section of the mean meridional wind (arrows) and mean zonal wind (isolines) along the meridian 30° E in the period 1–10 August 2010. The step of isolines is 5 m s^{-1} . Westerlies are depicted by solid contours while easterlies are dotted within the shaded region. Zero isoline is omitted. Large dots depict the tropopause position.

Thus, the increased WV content in the lower stratosphere might promote the decrease in ozone content and, as a consequence, the decrease in TCO.

An increase of WV content in the lower stratosphere could also intensify the chlorine catalytic cycle of ozone destruction. The rate of chlorine activation in heterogeneous reactions of HCl and ClONO₂ on aerosol particles and therefore the rate of ozone destruction by chlorine increases with temperature decreasing. In spite of the marked stratospheric cooling observed during the spring and summer 2010 atmospheric blocking periods (Fig. 6e), the lower-stratospheric temperatures over blocking regions remained higher than the threshold needed for the formation of polar stratospheric clouds: -80°C (Solomon et al., 1986). However, according to the Anderson et al. (2012) model results, an increase in stratospheric WV content raises the temperature threshold for the reactions and the activation of chlorine may take place at higher temperature even during the summer period for mid-latitudes. The role of heterogeneous photochemistry could increase also due to supply of smoke aerosol into the stratosphere from massive wildfires occurring within ER during this period. Assessments of the photochemical mechanism effectiveness and relative contributions of photochemical and dynamical processes involved in TCO decrease during atmospheric blocking require a more comprehensive study, including computational modeling.

5. Summary and conclusions

Using data from AIRS satellite instrument, the ozone and water vapor (WV) anomalies associated with the spring and summer atmospheric blocking events over European Russia (ER) during 2010 were analyzed. Within the domains of the blocking anticyclones, negative total column ozone (TCO) and positive total column water vapor (TCWV) anomalies were observed. These anomalies reached values of -25 and -33 DU (TCO) and 10 and 11 kg m^{-2} (TCWV) during the spring and summer, respectively. Over the regions up and downstream from the blocks, positive TCO anomalies (80 and 49 DU) and negative TCWV anomalies (-3 and -4 kg m^{-2}) were observed, respectively.

The TCO and TCWV anomalies were likely of dynamic origin and were associated with the large-scale atmospheric circulation accompanying an omega-type blocking. The TCO deficit and TCWV surplus over the blocking domains are explained primarily by the poleward advection of ozone depleted but WV-enriched subtropical air along the western and northern flanks of blocking anticyclones. Also, this scenario is associated with tropopause uplift. The most intense meridional transport of subtropical air occurred in the UTLS region, directly through the tropopause break. The TCO and TCWV anomalies found in the blocking anticyclone region over ER during the summer 2010 were linked also inherently to the global pattern of TCO and TCWV anomalies associated with a quasi-stationary Rossby wave train. The mechanism for the formation of the TCO and TCWV anomalies within the blocking domains also likely included the vertical motions inherent in planetary wave dynamics.

The increase in TCWV within the domains of blocks was due primarily to an WV increase in the lower troposphere. Additionally, a considerable increase in WV was found also in the upper troposphere and in the lower stratosphere and the WV increase was approximately 40% during both the blocking events. The increase in WV in the lower stratosphere over the blocking domains could contribute to ozone depletion due to the destruction of ozone in photochemical reactions involving WV.

Acknowledgements

The authors are grateful to the NASA AIRS science team and the NCEP/NCAR reanalysis group for the data used in this study. AIRS data were obtained via the Giovanni online data system, developed and maintained by the NASA GES DISC. This work was supported by the Russian Foundation for Basic Research (grant number 15-05-07853) and Russian Science Foundation (grant number 14-17-00806). The authors are also grateful to the anonymous reviewers for their time and effort, which made this paper stronger.

Appendix A. Supplementary data

Supplementary data related to this article can be found at <http://dx.doi.org/10.1016/j.atmosenv.2017.06.004>

References

- Acker, J.C., Leptoukh, G., 2007. Online analysis enhances use of NASA Earth science data. *Eos Trans. AGU* 88, 14–17. <http://dx.doi.org/10.1029/2007E0020003>.
- Anderson, J.G., Wilmouth, D.M., Smith, J.B., Sayres, D.S., 2012. UV dosage levels in summer: increased risk of ozone loss from convectively injected water vapor. *Science* 337 (6093), 835–839. <http://dx.doi.org/10.1126/science.1222978>.
- Aumann, H.H., Chahine, M.T., Gautier, C., Goldberg, M., Kalnay, E., McMillin, L., Revercomb, H., Rosenkranz, P.W., Smith, W.L., Staelin, D., Strow, L., Susskind, J., 2003. AIRS/AMSU/HSB on the Aqua mission: design, science objectives, data products, and processing systems. *IEEE Trans. Geosci. Remote Sens.* 41, 253–264. <http://dx.doi.org/10.1109/TGRS.2002.808356>.
- Barriopedro, D., Antón, M., García, G.A., 2010. Atmospheric blocking signatures in total ozone and ozone miniholes. *J. Clim.* 23, 3967–3983. <http://dx.doi.org/10.1175/2010JCLI3508.1>.
- Bekoryukov, V.I., 1965. On the theory of atmospheric ozone transfer in the presence of long waves. *Izv. Atmos. Ocean. Phys.* 1 (9), 897–905.
- Chahine, M., Pagano, T.S., Aumann, H.H., Atlas, R., Barnet, C., Blaisdell, J., Chen, L., Divakarla, M., Fetzer, E.J., Golberg, M., Gautier, C., Granger, S., Hannon, S., Irion, F.W., Kakar, R., Kalnay, E., Lambrigtsen, B.H., Lee, S.-Y., Le Marshall, J., McMillan, W.W., McMillin, L., Olsen, E.T., Revercomb, H., Rosenkranz, P., Smith, W.L., Staelin, D., Strow, L.L., Susskind, J., Tobin, D., Wolf, W., Zhou, L., 2006. AIRS improving weather forecasting and providing new data on greenhouse gases. *Bull. Am. Meteor. Soc.* 87 (7), 911–926. <http://dx.doi.org/10.1175/BAMS-87-7-911>.
- Huijnen, V., Flemming, J., Kaiser, J.W., Inness, A., Leitão, J., Heil, A., Eskes, H.J., Schultz, M.G., Benedetti, A., Hadji-Lazarou, J., Dufour, G., Eremenko, M., 2012. Hindcast experiments of tropospheric composition during the summer 2010 fires over western Russia. *Atmos. Chem. Phys.* 12 (9), 4341–4364. <http://dx.doi.org/10.5194/acp-12-4341-2012>.
- Hunt, B.G., 1966. Photochemistry of ozone in a moisture atmosphere. *J. Geophys. Res.* 71 (5), 249–254. <http://dx.doi.org/10.1029/JZ071i005p01385>.
- James, P.M., 1998. A climatology of ozone mini-holes over the Northern Hemisphere. *Int. J. Climatol.* 18, 1287–1303. [http://dx.doi.org/10.1002/\(SICI\)1097-0088\(199810\)18,12<1287](http://dx.doi.org/10.1002/(SICI)1097-0088(199810)18,12<1287).
- Kistler, R., Collins, W., Saha, S., White, G., Woollen, J., Kalnay, E., Chelliah, M., Ebisuzaki, W., Kanamitsu, M., Kousky, V., van den Dool, H., Jenne, R., Fiorino, M., 2001. The NCEP–NCAR 50-year reanalysis: monthly means CD-ROM and documentation. *Bull. Amer. Meteor. Soc.* 82, 247–267. [http://dx.doi.org/10.1175/1520-0477\(2001\)082<0247:TNNYRM>2.3.CO;2](http://dx.doi.org/10.1175/1520-0477(2001)082<0247:TNNYRM>2.3.CO;2).
- Koch, G., Wernli, H., Schwierz, C., Staehelin, J., Peter, T., 2005. A composite study on the structure and formation of ozone miniholes and minihighs over central Europe. *Geophys. Res. Lett.* 32, L12810. <http://dx.doi.org/10.1029/2004GL022062>.
- Lupo, A.R., Smith, P.J., 1995. Climatological features of blocking anticyclones in the Northern Hemisphere. *Tellus* 47A, 439–456. <http://dx.doi.org/10.1034/j.1600-0870.1995.t01-3-00004.x>.
- Lupo, A.R., Mokhov, I.I., Akperov, M.G., Chernokulsky, A.V., Athar, H., 2012. A dynamic analysis of the role of the planetary- and synoptic-scale in the summer of 2010 blocking episodes over the European part of Russia. *Adv. Meteorol.* 11. <http://dx.doi.org/10.1155/2012/584257>. Article ID 584257.
- Matsumoto, T., 1980. Lagrangian motion of air parcels in the stratosphere in the presence of planetary waves. *Pure Appl. Geophys.* 118, 189–216. <http://dx.doi.org/10.1007/BF01586451>.
- Mo, T., 1996. Prelaunch calibration of the advanced microwave sounding unit-a for NOAA-K. *IEEE Trans. Microw. Theory Techn* 44 (8), 1460–1469.
- Mokhov, I.I., 2011. Specific features of the 2010 summer heat formation in the European territory of Russia in the context of general climate changes and climate anomalies. *Izv. Atmos. Ocean. Phys.* 47 (6), 653–660.
- Mokhov, I.I., Timazhev, A.V., Lupo, A.R., 2014. Changes in atmospheric blocking characteristics within Euro-Atlantic region and Northern Hemisphere as a whole in the 21st century from model simulations using RCP anthropogenic

- scenarios. *Glob. Planet. Change* 122, 265–270. <http://dx.doi.org/10.1016/j.gloplacha.2014.09.004>.
- Orsolini, Y., Nikulin, G., 2006. A low-ozone episode during the European heatwave of August 2003. *Q. J. R. Meteorol. Soc.* 132, 667–680. <http://dx.doi.org/10.1256/qj.05.30>.
- Pagano, T.S., Chahine, V.T., Fetzer, E.J., 2010. The Atmospheric Infrared Sounder (AIRS) on the NASA Aqua spacecraft: a general remote sensing tool for understanding atmospheric structure, dynamics and composition. *Proc. SPIE* 7870 (78270B), 1–8. <http://dx.doi.org/10.1117/12.865335>.
- Pelly, J.L., Hoskins, B.J., 2003. A new perspective on blocking. *J. Atmos. Sci.* 60 (3), 743–755. [http://dx.doi.org/10.1175/1520-0469\(2003\)060<0743:ANPOB>2.0.CO;2](http://dx.doi.org/10.1175/1520-0469(2003)060<0743:ANPOB>2.0.CO;2).
- Perov, S.P., Khrgian, A.Kh., 1980. *The Modern Problems of Atmospheric Ozone. Hydrometeoizdat, Leningrad* (in Russian).
- Peters, D., Egger, J., Entzian, G., 1995. Dynamical aspects of ozone mini-hole formation. *Meteorol. Atmos. Phys.* 55, 205–214. <http://dx.doi.org/10.1007/BF01029827>.
- Petzold, K., 1999. The role of dynamics in total ozone deviations from their long-term mean over the Northern Hemisphere. *Ann. Geophys.* 17, 231–241. <http://dx.doi.org/10.1007/s00585-999-0231-1>.
- Petzold, K., Naujokat, B., Neugeboren, K., 1994. Correlation between stratospheric temperature, total ozone and tropospheric weather systems. *Geophys. Res. Lett.* 21, 1203–1206. <http://dx.doi.org/10.1029/93GL03020>.
- Rex, D.F., 1950. Blocking action in the middle troposphere and its effect on regional climate. *Tellus* 2, 275–301. <http://dx.doi.org/10.1111/j.2153-3490.1950.tb00331.x>.
- Shakina, N.P., Ivanova, A.R., 2010. Blocking anticyclones: current state of investigations and forecasting. *Russ. Meteorol. Hydrol.* 35 (11), 721–730. <http://dx.doi.org/10.3103/S1068373910110014>.
- Sitnov, S.A., 2011a. Satellite monitoring of atmospheric gaseous species and optical characteristics of atmospheric aerosol over the European part of Russia in April–September 2010. *Dokl. Earth Sci.* 437 (1), 368–373. <http://dx.doi.org/10.1134/S1028334X11030081>.
- Sitnov, S.A., 2011b. Spatial-temporal variability of the aerosol optical thickness over the central part of European Russia from MODIS data. *Izv. Atmos. Ocean. Phys.* 47 (5), 584–602. <http://dx.doi.org/10.1134/S0001433811050100>.
- Sitnov, S.A., Mokhov, I.I., 2013. Water-vapor content in the atmosphere over European Russia during the Summer 2010 fires. *Izv. Atmos. Ocean. Phys.* 49 (4), 414–429. <http://dx.doi.org/10.1134/S0001433813040099>.
- Sitnov, S.A., Mokhov, I.I., 2015. Ozone mini-hole formation under prolonged blocking anticyclone conditions in the atmosphere over European Russia in summer 2010. *Dokl. Earth Sci.* 460 (1), 41–45. <http://dx.doi.org/10.1134/S1028334X15010067>.
- Sitnov, S.A., Mokhov, I.I., 2016. Satellite-derived peculiarities of the spatial distribution of total ozone under atmospheric blocking conditions over the European part of Russia in summer of 2010. *Russ. Meteorol. Hydrol.* 41 (2), 28–36. <http://dx.doi.org/10.3103/S1068373916010040>.
- Sitnov, S.A., Mokhov, I.I., 2017. Formaldehyde and nitrogen dioxide in the atmosphere during summer weather extremes and wildfires in European Russia in 2010 and Western Siberia in 2012. *Intern. J. Remote. Sens.* 38 (14), 4086–4106. <http://dx.doi.org/10.1080/01431161.2017.1312618>.
- Sitnov, S.A., Mokhov, I.I., Lupo, A.R., 2014. Evolution of water vapor plume over Eastern Europe during summer 2010 atmospheric blocking. *Adv. Meteorol.* 11. <http://dx.doi.org/10.1155/2014/253953>. Article ID 253953.
- Solomon, S., Garcia, R.R., Rowland, F.S., Wuebbles, D.J., 1986. On the depletion of Antarctic ozone. *Nature* 321, 755–758. <http://dx.doi.org/10.1038/321755a0>.
- Stick, C., Kruger, K., Schade, N.H., Sandmann, H., Macke, A., 2006. Episode of unusual high solar ultraviolet radiation over central Europe due to dynamical reduced total ozone in May 2005. *Atmos. Chem. Phys.* 6, 1771–1776. <http://dx.doi.org/10.5194/acp-6-1771-2006>.
- Susskind, J., Barnett, C., Blaisdell, J., Iredell, L., Keita, F., Kouvaris, L., Molnar, G., Chahine, M., 2006. Accuracy of geophysical parameters derived from Atmospheric Infrared Sounder/Advanced Microwave Sounding Unit as a function of fractional cloud cover. *J. Geophys. Res.* 111, D09S17. <http://dx.doi.org/10.1029/2005JD006272>.
- Tian, B., Manning, E., Fetzer, E.J., Olsen, E., Wong, S., Susskind, J., Iredell, L., 2013. AIRS/AMSU/HSB Version 6 Level 3 Product User Guide. http://disc.sci.gsfc.nasa.gov/AIRS/documentation/v6_docs/v6releasedocs-1/V6_L3_User_Guide.pdf.
- Tibaldi, S., Molteni, F., 1990. On the operational predictability of blocking. *Tellus* 42A, 343–365. <http://dx.doi.org/10.1034/j.1600-0870.1990.t01-2-00003.x>.
- van Donkelaar, A., Martin, R.V., Levy, R.C., da Silva, A.M., Krzyzanowski, M., Chubarova, N.E., Semutnikova, E.G., Cohen, A.J., 2011. Satellite-based estimates of ground-level fine particulate matter during extreme events: a case study of the Moscow fires in 2010. *Atmos. Environ.* 45, 6225–6232. <http://dx.doi.org/10.1016/j.atmosenv.2011.07.068>.
- Wiedenmann, J.M., Lupo, A.R., Mokhov, I.I., Tikhonova, E.A., 2002. The climatology of blocking anticyclones for the Northern and Southern Hemispheres: block intensity as a diagnostic. *J. Clim.* 15, 3459–3473. [http://dx.doi.org/10.1175/1520-0442\(2002\)015<3459:TCOBAF>2.0.CO;2](http://dx.doi.org/10.1175/1520-0442(2002)015<3459:TCOBAF>2.0.CO;2).
- Witte, J.C., Douglass, A.R., da Silva, A., Torres, O., Levy, R., Duncan, B.N., 2011. NASA A-Train and Terra observations of the 2010 Russian wildfires. *Atmos. Chem. Phys.* 11, 9287–9301. <http://dx.doi.org/10.5194/acp-11-9287-2011>.
- World Meteorological Organization, 1957. *WMO Bull.* 6 (4), 134–138. https://library.wmo.int/pmb_ged/bulletin_6-4_en.pdf.